Results from a scaled final focus experiment for heavy ion fusion

S. A. MacLaren[a)]
Lawrence Livermore National Laboratory, L-015, 7000 East Avenue, Livermore, California 94550

A. Faltens and P. A. Seidl
Lawrence Berkeley National Laboratory, Mailstop 47-112, One Cyclotron Road, Berkeley, California 94720

D. V. Rose
Mission Research Corporation, 5001 Indian School Road, NE Albuquerque, New Mexico 87110-3946

(Received 12 October 2001; accepted 1 February 2002)

A one-tenth-scale version of a final focus subsystem for a heavy-ion-fusion driver has been built and used for experimental tests of concept. By properly scaling the parameters that relate ion energy and mass, current, emittance, and focusing fields, the transverse dynamics of a representative driver final focus have been replicated in a small laboratory beam. Whereas the driver beam parameters considered are 10 GeV Bi^+ at 1.25 kA, the scaled experiment used a 95 μA beam of 160 keV Cs^+ ions brought to a ballistic focus through a series of six quadrupole magnets. The measured focal spot size was consistent with calculations in the report of the design on which the experiment is based. In a second experimental program, a 400 μA beam was propagated through the focal system and partially neutralized after the last magnet using electrons released from a hot tungsten filament to test the predictions of the benefits of neutralization. The increase in beam current resulted in a corresponding increase in spot radius in the absence of electrons. A reduction of the spot radius and modification of its shape were observed in the presence of neutralizing electrons. [DOI: 10.1063/1.1464894]

I. BACKGROUND AND MOTIVATION

Due to the high repetition rate and predicted high efficiency of particle accelerators, intense heavy ion beams are a promising driver for an inertial confinement fusion power plant.[1,2] The final focus subsystem must deliver the accelerated beams to the fusion target in a precise and symmetric fashion, overcoming the forces within the beam that tend to resist focusing. Because the ions in a driver are only marginally relativistic ($\beta = 0.2-0.3$), the magnetic pinch force is an order of magnitude weaker than the electrostatic space charge force pushing radially outward on the beam. Additionally, there is thermal velocity spread, or emittance, in the transverse plane that will put a lower bound on the spot radius. Finally, aberrations resulting from imperfections in the focusing field as well as deviations from the nominal beam momentum affect the spot size, shape, and location.

Final focus designs generally fall into three categories with varying uncertainty surrounding issues of physics: (i) Un-neutralized (high vacuum) ballistic focusing is the most straightforward method in the context of accelerator physics, relying on the transverse momentum imparted to the ions by the focusing fields to produce trajectories that will overcome the forces mentioned above and result in a satisfactory focal spot.[3] (ii) Ballistic focusing with neutralization uses electrons from external sources to partially overcome the space charge force.[4] In this manner, a lower ion kinetic energy and higher beam current may be used, preserving both the total beam energy and focal spot size. (iii) Finally, there are other proposed forms of nonballistic focusing generally referred to as channel transport.[5,6] This category includes methods that employ an electrical discharge or self-pinch in a gas to maintain the beam at small radius in a ''channel'' through the chamber to the target. While these classes of designs are listed in order of increasing complexity with respect to the plasma physics, they are in decreasing order of difficulty in the phase space and ion kinetic energy constraints placed on the ion beam delivered by the accelerator. This contrast demonstrates a tradeoff between issues of cost and uncertainties in the beam dynamics that play an important role in the design of a heavy ion fusion power plant final focus subsystem and target chamber.

The Scaled Final Focus Experiment at Lawrence Berkeley National Laboratory (LBNL) models the final focus subsystem of the HIBALL-II (Ref. 7) power plant design, which assumes un-neutralized ballistic focusing. The configuration is relatively straightforward, consisting of six magnetic quadrupoles, with the final magnet located immediately outside the fusion chamber. Such a system is well suited to an initial experimental verification of the effectiveness of a final focus method. By properly scaling the parameters that relate particle energy and mass, beam current, beam emittance, and focusing field, we replicate the dynamics of a full driver beam in a small laboratory beam. This is the first experimental test, appropriately scaled from a specific heavy ion driver design, of the beam dynamics involved with focusing ions onto the fusion target. As such, it includes many of the more complex effects (e.g., nonuniformities in the phase space distribution and end effects associated with the magnetic qua-

a)Author to whom correspondence should be addressed. Electronic mail: maclaren2@llnl.gov

drupoles) that often raise questions when it is not practical to consider them in theoretical studies.

Studies of ion beam propagation through the fusion chamber indicate that there exist a number of possible mechanisms for production of electrons that could interact with the beam. Electric field induced emission at the beam entrance port, ionization of background gas, and photoionization of the beam and gas by the heated target can all contribute electrons that will make some degree of neutralization unavoidable.[8–10] Additionally, an optimization of the final ion energy for a power plant will consider the effect of a reduction of the ion energy not only on the cost of the accelerator, but also on the effect in the target radiator due to the resulting shortening of the ion range. The design energy may well be lower than the value at which the ballistic ion trajectories alone can produce a satisfactory spot radius.

In light of these considerations, the LBNL experiment also studied the addition of electrons to a beam whose space charge forces were large enough to prevent the scaled ballistic focus from achieving a useful focal spot size. In this case, introducing these electrons resulted in a transition from a space-charge-dominated to an emittance-dominated focus. The effective and uniform neutralization observed provided a low current test of some of the basic physics issues involved with electron neutralization of a converging beam of heavy ions.

II. SCALING THE FOCUS

Proper scaling of the beam current, external focusing gradients, and emittance with the beam energy and dimensions is critical to reproduce the particle trajectories of a full scale driver in a small laboratory experiment. The scaling is evident in the beam envelope equation, which gives the trajectory of the edge of the beam as a function of the self generated and applied fields and the emittance. This equation, along with the a phase space distribution function describing a beam that obeys the equation, was first derived by Kapchinskij and Vladimirskij[11] subject to several important assumptions. The axial velocity of the particles, v, is assumed to be constant and large compared to the radial and azimuthal velocities, consistent with the paraxial approximation. The beam charge density is taken to be uniform, filling an elliptical cross section with semiaxes a and b. Together these assumptions describe a constant line charge density, λ, and result in linear self-fields within the beam. The axial beam dimension is assumed to be much longer than the radii, $l \gg a,b$, and the beam is composed entirely of particles with a single mass m and charge e (charge state $+1$).

With these assumptions, the beam's transverse self-fields in free space are

$$\mathbf{E}=\frac{\lambda}{\pi\varepsilon_0}\frac{1}{a+b}\left(\frac{x}{a}\hat{a}+\frac{y}{b}\hat{y}\right), \tag{1}$$

$$\mathbf{B}=\frac{\mu_0\lambda}{\pi}v\frac{1}{a+b}\left(-\frac{y}{b}\hat{x}+\frac{x}{a}\hat{y}\right) \tag{2}$$

for $0\leqslant x\leqslant a$ and $0\leqslant y\leqslant b$, and the equation of motion in the x direction for a single particle becomes

$$\ddot{x}=\frac{e}{\gamma m}[E_x(z)-vB_y(z)]_{\text{ext}}+\frac{e}{\gamma m}\frac{\lambda}{\pi\varepsilon_0}\frac{1}{a+b}\left(1-\frac{v^2}{c^2}\right)\frac{x}{a}, \tag{3}$$

where the first term denotes the external focusing force from either electrostatic or magnetic quadrupoles. With time independent, the time derivative is converted to a derivative with respect to z (the $'$ notation will be used to indicate the z derivative)

$$x''+k_x(z)x-\frac{eI}{\pi\varepsilon_0 m(\beta\gamma c)^3}\frac{1}{a(a+b)}x=0, \tag{4}$$

where the external quadrupolar electrostatic and magnetic focusing fields are represented by

$$k_x(z)=\frac{e}{\gamma m v^2}\frac{dE_x(z)}{dx},\quad -\frac{e}{\gamma m v}\frac{dB_y(z)}{dx},$$

respectively. The solution for the resulting differential equation for x can be written in the form,[12]

$$x=\sqrt{\varepsilon_x}w(z)\cdot\cos\Psi(z),$$

where $\Psi'=w^{-2}(z)$. The emittance, ε_x, is a constant of the motion that is related physically to $x\cdot p_x$, the area of the projection of the six-dimensional phase space volume along the transverse coordinate. It is conserved due to the linear forces arising from the uniform charge density of the phase space distribution. Substitution of this solution into Eq. (4) results in an expression for w that can be evaluated at the edge radius a, i.e., $a=\sqrt{\varepsilon_x}w(z)$,

$$a''=k_x(z)a+\frac{2Q}{a+b}+\frac{\varepsilon_x^2}{a^3}. \tag{5}$$

Here, $Q=eI/2\pi\varepsilon_0 m(\beta\gamma c)^3$ is the (dimensionless) perveance.

For the evaluation of experimental data, a rms expression for ε_x is derived via the rms envelope radius, defined as $\langle x^2\rangle=a^2/4$. We take derivatives of this relation and then insert the equation of motion for a particle in the x direction [Eq. (4)] into the second derivative. The result can be compared to the envelope equation [Eq. (5)] to yield a quantity that may be readily extracted from the experimental data,

$$\varepsilon_{x\text{edge}}=4\varepsilon_{x\text{rms}}=4\sqrt{\langle(x')^2\rangle\langle x^2\rangle-\langle xx'\rangle^2}. \tag{6}$$

Scaling the experiment is necessary due to the laboratory constraints; both the physical size of the design's final focus section and the final energy of the ions are beyond the capacities of the experimental facility. This scaling is accomplished so as to maintain the relative strengths of the terms in Eq. (5), and therefore preserve the particle trajectories through the system. The ~100 m magnetic final focus section of the HIBALL-II study has been reproduced in the laboratory at one-tenth scale, so that the quantities with the dimension of length (spot radius and emittance) are reduced by this scale factor of 10. The Cs^+ ion beam is launched with a 160 kV pulse from a Marx generator, and the beam current and magnetic focusing fields are then chosen so that the self-force and external-focusing-force terms keep their relative strengths, respectively. Of course, dimensionless quantities

such as the final convergence angle and the beam perveance are preserved from the design to the experiment.

To match the perveance of the 10 GeV Bi^+ beam at 1.25 kA in the study, the 160 keV experimental beam is apertured to extract 95 μA. The scaled values of the pole tip fields in the six focusing magnets range from 200 to 600 G. A high brightness Cs^+ ion source, designed specifically for the experiment, delivers an un-normalized emittance of 4 π mm mrad following the aperture, in fairly good agreement, once scaled, to the value of 30 π mm mrad reported in Ref. 7. The details of these scaling calculations are found in Ref. 15.

The envelope equation can also be used to predict the minimum radius of the beam for a given convergence angle from the last focusing element. First, we write Eq. (5) for a round beam of radius r in a region with no external focusing fields,

$$r''=\frac{Q}{r}+\frac{\varepsilon_x^2}{r^3}. \tag{7}$$

We multiply by r' and integrate along the axial direction until the radius reaches a minimum at $r_f'=0$. Noting that $r_o'=\theta$ (convergence angle), and that θ and the initial radius are related by the focal length L, an expression that contains the focal spot size is

$$\theta^2-\left(\frac{\varepsilon_x^2}{r_f^2}-\frac{\varepsilon_x^2}{r_i^2}\right)=2Q\ln\left(\frac{\theta L}{r_f}\right). \tag{8}$$

In the limits $r_i \gg r_f$ and $\varepsilon^2/r_f^2 \gg Q$, an approximate formula is obtained for an emittance dominated focus,

$$r_f \cong \frac{\varepsilon}{\theta}. \tag{9}$$

This relation illustrates the importance of the emittance in determining the spot size and therefore the specific energy deposited on the target. For a convergence angle that minimizes the effects of geometric aberrations ($\theta \leqslant 20$ mrad),[13] the emittance available from the accelerator is balanced against the desired focal spot parameters of the target. The opposite limit is that of a space charge dominated focus, which would result from the higher current, lower kinetic energy conditions discussed in Sec. I. Addressing the issue of handling these higher perveance beams through designs that employ partial or full neutralization is an area of active research.[8,9,14] The goal of these efforts is to return the focal spot to the regime in which the radius is determined only by the emittance and convergence angle at the final focus. Therefore, Eq. (9) often serves as a parametric constraint for optimizing driver designs.[4]

III. DESCRIPTION OF THE EXPERIMENT

The main components of the Scaled Final Focus Experiment are an ion source and its high voltage pulser, an electrostatic section for the selection of the scaled current and preparation of the beam, and a magnetic section that closely follows the full-scale design. The single deviation from the HIBALL-II layout is the length of the drift section between the third and fourth magnets; it has been shortened to allow for a more compact experimental apparatus. The monoenergetic beam is low in perveance ($Q=1.1\times10^{-5}$); therefore, the sole effect on the beam dynamics of shortening the middle drift in the magnetic section is a slight adjustment to the beam envelope at the exit of the third quadrupole. The components are enclosed by a vacuum system accommodating numerous feedthroughs for electrical connections and beam diagnostics. A rotating wheel containing a number of apertures is located between the source and electrostatic section and was used to select the beam current without needing to open the vacuum enclosure. A schematic of the apparatus is shown in Fig. 1.

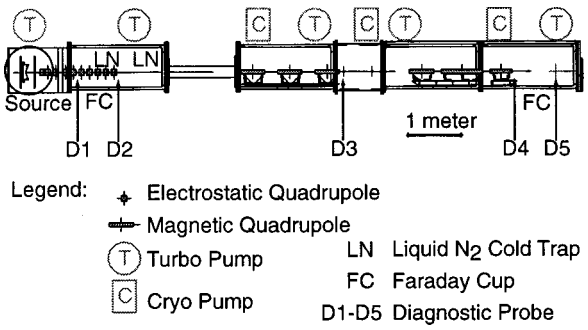

FIG. 1. Layout of the scaled final focus experiment.

Following the aperture is a 1.6 m lattice of ten electrostatic quadrupoles with independently controlled voltages, and slit scanner diagnostics after the fifth and tenth quadrupoles. This lattice served to match the apertured beam size and convergence angle into the drift preceding the final focus magnet lattice. The magnetic focusing section is 8.2 m long (including initial and final drifts) and includes diagnostics after the third and sixth magnets. Additionally, there is a slit-cup probe located 0.8 m beyond the last magnet to measure the properties of the focal spot. The magnets are iron-free, pulsed quadrupoles, and consist of two layers of copper windings in an azimuthal distribution that best approximates a $\cos(2\theta)$ surface current. The windings were epoxied into groves cut into cylindrical Lexan shells; a schematic is shown in Fig. 2. Each of the magnet inner diameters was lined with a grounded metal foil to simulate the beam pipe in the design focusing system. Because each magnet has a rise-time characteristic of its inductance, the triggers were appropriately delayed to synchronize the current waveform flattop with the arrival of the beam.

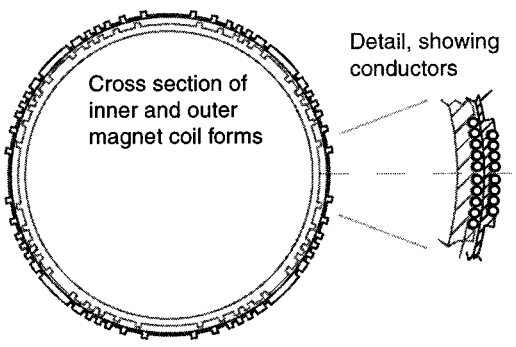

FIG. 2. Inner and outer coil forms used to position the magnetic quadrupole windings.

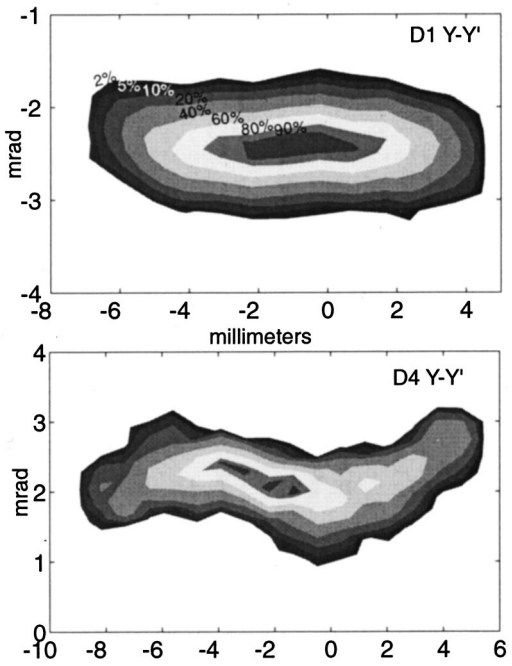

FIG. 3. $Y-Y'$ projections of phase space measured at the $D1$ and $D4$ locations.

Each diagnostic location consists of at least one pair of automated slit scanner probes. The downstream paddle in each pair has a shallow ($\sim$1 cm deep) collector cup mounted to the back of the slit. An isolated, positively biased mesh is located between the slit and the negatively biased collector, serving to amplify the incident ion signal with current from the secondary electrons. The slit cup paddle by itself measures the transverse current density profile of the beam. Parallel slits are used to measure the phase space density and emittance of the beam. Examples of this type of measurement made at D1 and D4 are shown in Fig. 3, where the phase space distribution of the beam is described by a set of intensity contours. Slits oriented perpendicular to each other can be used to map out the current density in the $X-Y$ plane. The focal spot probe uses two orthogonal slit cup assemblies mounted on a platform that translates along all three axes, such that beam spot profiles can be measured at various axial locations. Each of these measurements is automated and computer controlled, including triggering the source diode pulse, moving the probes, and extracting and storing the measured waveforms from a digitizing oscilloscope.

There are two Faraday cups for measurement of the total beam current and transmission through the final focus lattice; one could be inserted in place of the seventh and eighth electrostatic quadrupoles, and the other into the drift after the last magnet. Co-located with this second Faraday cup is a capacitive drift tube diagnostic that was used to measure the total charge of the incident beam, and through comparison of several measurements, the fractional neutralization.

When the slits were in a position during the scan where there is no beam signal present, a certain level of noise was collected by the diagnostic. If this phase space location is particularly far from the centroid of the data, the noise could weigh heavily into the calculation of the second moments. It

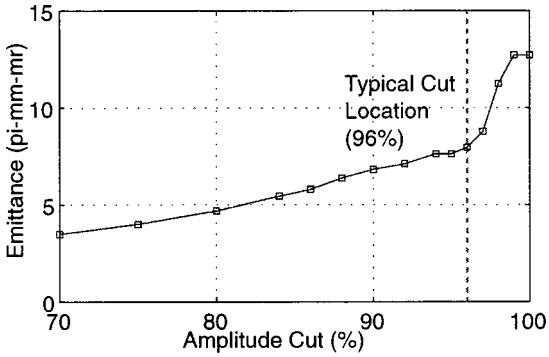

FIG. 4. Example of a cutoff used in an emittance calculation from experimental data.

is therefore useful to be able to exclude from the calculation a known fraction of the data whose amplitude lies below a given threshold. Without background noise, a plot of calculated emittance vs percent signal included would produce a smooth function to 100%. A plot of actual data on the same axes is shown in Fig. 4, indicating the sharp break in the slope of the data due to the presence of the noise. The emittance measurements considered in this paper and used in beam dynamics calculations are based on a cut made in the manner of Fig. 4, with the signal included in the calculation typically 95% of the total collected during the scan.

IV. BALLISTIC FOCUS AND CHROMATIC EFFECTS

The ballistic focus that is described in the HIBALL-II report brings the 1.25 kA beam of 10 GeV Bi^+ ions to a spot with a 9 mrad convergence angle. By reproducing the trajectories of the ions in this focusing system, the experiment preserves this convergence angle and attempts to achieve a focal spot with transverse dimensions one-tenth that of the design. Given the beam parameters at the end of the final focus subsystem, an analytic prediction of the minimum radius or focal spot size of the beam can be made as described in Sec. II. For the HIBALL-II design, one arrives at 5.8 mm for a twice rms spot radius, and therefore a goal of 0.58 mm for the scaled experiment.[15]

The nature of the transverse beam distribution at the focal spot is determined by the self-forces that oppose the inward momentum imparted to the ions by the net effect of the quadrupole magnets. Because the emittance term in the envelope equation is approximately six times stronger than the space charge term at the focus, the beam's transverse thermal momentum spread will result in a radial density profile that is Gaussian in shape.[16] Assuming a two-dimensional Gaussian distribution with $\sigma=0.29$ mm for the scaled HIBALL-II focal spot, a fraction-vs-radius curve can be generated by numerically integrating this distribution at a series of radii. This representation of beam current fraction vs spot radius is plotted with a solid line in Fig. 5.

The focal spot measurements consist of transverse slit scans that project the beam current density distribution onto either of the transverse axes as shown in Fig. 6. Therefore, it is not possible to plot an unambiguous representation of the fraction of the experimental current that falls within a given

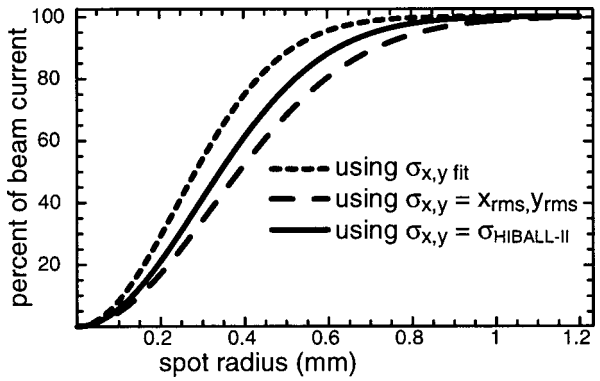

FIG. 5. Percent of beam current at the focus as a function of radius assuming a two-dimensional Gaussian distribution.

radius. However, a Gaussian radial density profile projected onto one axis by the slit scan results in a measured profile that is also Gaussian with the same σ. The slit scan data at the focus are fit with a Gaussian curve in order to extract this value of σ, shown in the figure. Asymmetries were present in both transverse planes; however, the horizontal asymmetry appears to be more severe in the figure. In the fifth magnet, the beam underwent its largest envelope excursion in the horizontal plane, allowing this plane to sample the most nonlinear portion of the quadrupole field. This effect, coupled with the small beam centroid asymmetries present throughout the magnetic section, tended to consistently degrade the measurements of the horizontal focus.

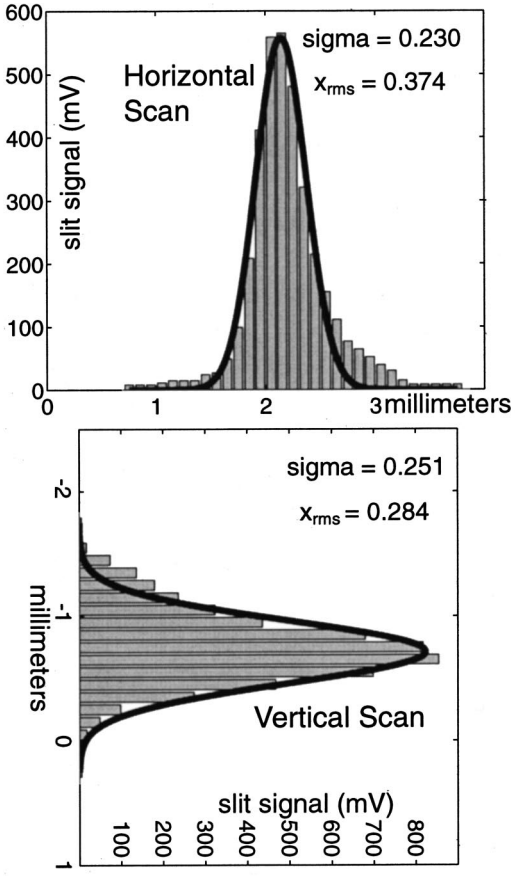

FIG. 6. Single slit profiles of the 95 μA ballistic focus.

Assuming that the current density at the spot has a two-dimensional Gaussian form with the fit values of σ as independent widths in the x and y transverse dimensions, the integration described above to generate the scaled HIBALL-II result is performed on this representation and the results plotted as the dotted curve in Fig. 5. Additionally, the second moment of the raw data can be used to calculate a rms radius for the measurements as indicated in Fig. 6. These radii can then serve as the x and y widths of a two-dimensional Gaussian distribution large enough to enclose virtually all of the data. The result of this calculation yields the dashed curve in Fig. 5. While the dotted curve resulting from Gaussian fits to the measured spot represents an idealized or ''best case'' scenario for the experiment, the dashed curve represents the lower bound or maximum radial extent of the distribution. Were a full two-dimensional measurement of the current density at the focal spot possible, the actual data would lie between the two curves. This is precisely where the HIBALL-II scaled design goal is found.

To study the effect of chromatic aberration on the above result, it would be desirable to adjust the beam energy at the few percent level holding all other parameters fixed. The experimental beam would then represent a transverse ''slice'' of a driver beam with each particle having the same value of energy deviation. However, Child's Law[17] governing extraction of ions from the source states that the beam current will increase as $V_{\mathrm{diode}}^{3/2}$. Also, one would want to vary the energy only in the magnetic section to prevent the effects of an energy shift in the electrostatic section from confusing the results. To avoid these issues, an energy shift was studied with the experiment by detuning the focusing gradients in a uniform manner. That is, the strengths of the pole tip fields in each of the six magnets were changed by the same fraction to simulate the deviation in beam energy.

In the experiment, measurements were made using the 95 μA beam with the magnetic quadrupole strengths detuned by $\pm 0.5\%$, and $\pm 1.0\%$, corresponding to energy shifts of $\pm 1\%$, and $\pm 2\%$. Because the target location in a fusion chamber would be fixed in space, the beam horizontal and vertical profiles were measured at the same axial location as in the nominal energy case. Figure 7 shows the fractional increase in the area of the focal spot for each of the cases. The light gray bars are the experimental measurements comparing the product of the widths of both planes to the product for the nonshifted ''on-momentum'' case.

Actually, the beam self-forces are also affected by a shift in energy. For this experiment, however, both the emittance and the perveance terms are small compared to the external focusing force term when the beam is in the magnets. This assumption was verified by modeling the chromatic effect in an envelope code that allows for both a uniform adjustment to the magnet strength as was done in the experiment and a real energy shift. The dark gray bars in Fig. 7 represent the calculated spot that results when each of the magnet strengths is shifted, and the medium gray bars are for the focus of a beam with the corresponding energy deviations. The agreement between the two models implies that the ef-

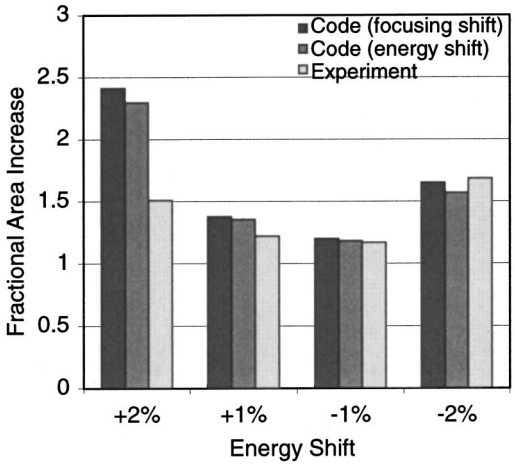

FIG. 7. Fractional increase in focal spot area for each of the energy shift trials.

fect of the energy shift on the forces other than the external focusing force is a small one for the given system.

From the figure, we see that the $\pm 1\%$ energy shifts increased the spot size by approximately 20%, and the $\pm 2\%$ by 50%–70%. The data is in fairly good agreement with the calculations of the code, except for the $+2\%$ case. For this case, the simulated beam passes through the horizontal focus several centimeters upstream of the measurement plane, and the calculated horizontal envelope is diverging rapidly at the point of measurement. Because this horizontal envelope minimum occurs in the code at a single point in z, the envelope equation predicts a large divergence in that plane downstream of the focus resulting in a large horizontal footprint at the measurement location. Distortions in the phase space of the experimental beam like those seen in Fig. 3, however, tend to spread out the focal waist in z, resulting in a smaller effective divergence angle of the envelope from the focal point. This detail may have a role in the discrepancy.

The results of a similar study of chromatic shifts are discussed in the HIBALL-II report. Here, the ion optics code used for the design of the final focus system tracked a monochromatic beam through the lattice at a series of energies.[7] The results are plotted as a fraction of the current that strikes within the desired radius (4 mm) compared to the on-momentum case. To plot the experimental results on the same axes, a Gaussian distribution is constructed based on the second moments of the focal spot data in each plane as is done for the dotted curve of Fig. 5 ($\sigma_{x,y}$ fit). For each of the momentum variations, the distribution based on the measurements is integrated out to the equivalent scaled radius (0.4 mm). To obtain an ''efficiency'' value, the result was normalized to the integral of the on-momentum data to the same radius. These calculations, along with the data from the HIBALL-II report are presented in Fig. 8. The experimental results, analyzed with the assumption of a two-dimensional Gaussian at the focus, appear to be less sensitive to the chromatic effects.

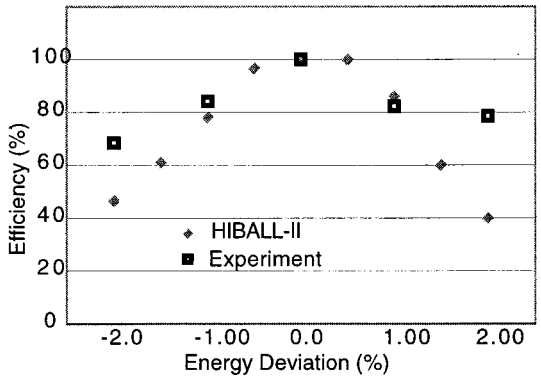

FIG. 8. The fraction of the current within a 0.4 mm radius is normalized to the on-momentum measurement and plotted as ''Efficiency'' for comparison to the HIBALL-II report.

V. NEUTRALIZED FOCUS

Using the envelope modeling code described in the previous section, it is found that by doubling the current limiting aperture radius, the resulting ~ 400 μA beam is just contained by the apertures and strengths of the focusing elements with a small margin (~ 3 mm) to avoid scraping. Using the emittance of this beam and holding the convergence angle to the focal point fixed at 9 mrad, the focal spot radius is plotted as a function of beam current at the focus in Fig. 9. The gray curve represents the values of spot radius where the space charge and emittance forces are equal. Without neutralization, the space charge force at the focal spot is five times larger than the emittance force, resulting in a 2.6 mm radius spot. Assuming a uniform density beam at the exit of the last magnet, the unneutralized spot will have a nearly uniform radial density profile. Following the black curve, addition of electrons to neutralize the space charge by 75% will shrink the spot radius to 1.25 mm and shift the focus across the gray curve into the emittance dominated regime. Thus, both the size and shape of the focal spot should change measurably.

Experimentally, neutralization of the higher current beam was accomplished with electrons emitted from a 75 μm diam hot ($\sim 2100\,^{\circ}$C) tungsten filament located after the last magnetic quadrupole, with $<1\%$ of the beam intercepted

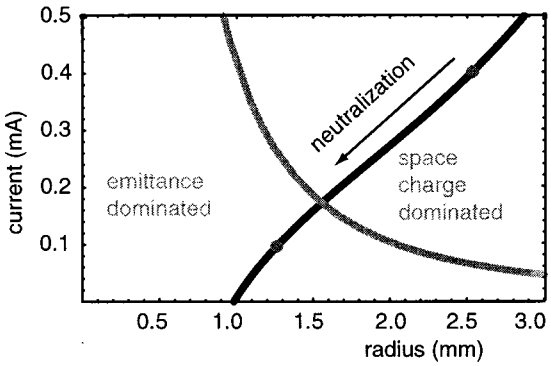

FIG. 9. Spot radius is plotted as a function of beam current leaving other parameters fixed, with the two points indicating the experimental values of the current. The light gray curve separates the emittance and space charge dominated regimes.

by the filament. Viewed in the beam frame, electrons born at the filament in the presence of the beam are trapped within the space charge potential ϕ of the beam only if $e\phi > \frac{1}{2}m_e v_{\text{beam}}^2$.[18] Treating the beam in the drift to the focus as a uniform cylinder of charge, the potential across the beam is approximately $\phi \approx 30I/\beta$. For the experiment, the beam space charge potential is approximately 7.5 V, while $\phi_{\min}$, the smallest potential that will still trap electrons, is 0.7 V. The maximum expected fractional neutralization is therefore ~90%. To eliminate the influence of the electrical potential across the filament, the heating power supply was switched via a solid state relay such that the potential on the filament was zero 500 μs prior to the arrival of the beam

The first of two measurements to determine the fractional neutralization was made with the drift tube diagnostic mentioned in Sec. II. As the beam approached the tube, a negative image charge resulted in current flow from the tube. This signal was measured and integrated to yield a waveform proportional to the charge present in the drift tube as a function of time. This waveform was observed to have the same characteristic shape as the beam current waveform that was recorded as the ions strike the collector of the Faraday cup. Therefore, the current measurement made at the Faraday cup at the same axial location as the drift tube was used as a reference for the integrated tube waveforms. The tube signal was acquired and scaled to match the Faraday cup signal, and comparison with an un-neutralized trial (filament removed) yields a neutralization fraction of 64%.

The measurements of the focal spot presented in Fig. 10 are slit scan profiles of the type discussed in the previous section, with each of the four measurements (horizontal and vertical scans, neutralized, and un-neutralized beams) made at the same axial location. These scans were made using a 50 μm slit with a 100 μm step size for the neutralized focus and a 250 μm step size for the case without neutralization. To emphasize the shift in the size and current density distribution of the focus, the neutralized profiles are fit with Gaussian curves. The values of σ shown on each plot represent the value from the fit to the data in the case of the neutralized beam spot. The Gaussian nature of the neutralized density is clear; the vertical fit is extremely good, but the horizontal fit is affected by the asymmetry in the profile. From these plots, the transition shown graphically in Fig. 9 from space charge dominated to emittance dominated focus is made clear.

To independently infer the fractional neutralization from these measurements, a comparison was made between the data and the envelope modeling code. The beam radii, convergence angles, and emittance measured at the exit of the last magnet were input as initial conditions, and the experiment was modeled using the full current to represent the results measured without neutralization. The beam current was then reduced until the resulting spot agrees with the neutralized measurements. The two cases are illustrated in Fig. 11. The fractional neutralization is then the ratio of the difference in current to the full current, 80% in this case.

To examine the conclusion that the changes in the measured characteristics of the focal spot are due to the acquisition of cold (~0.2 eV) electrons from the filament, the portion of the experiment from the filament to the focus was

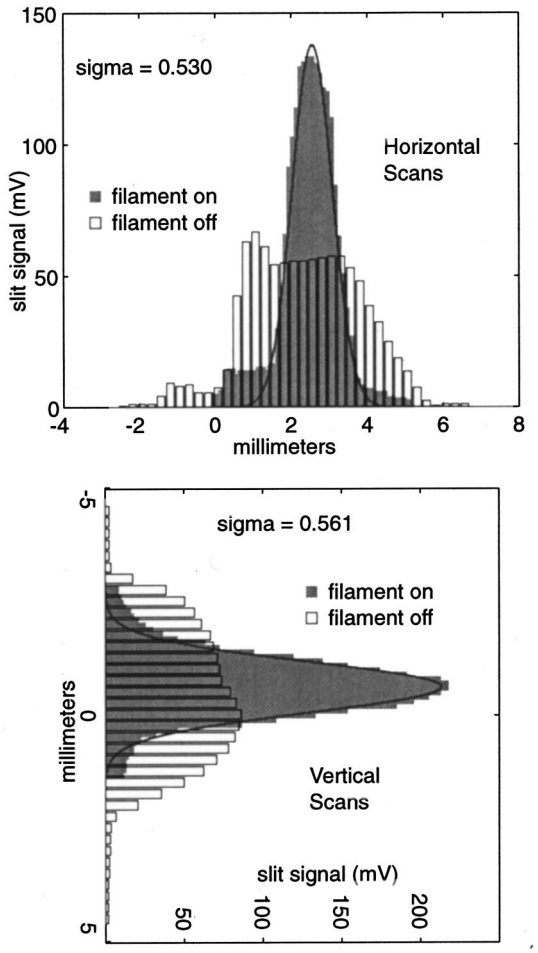

FIG. 10. Single slit profiles of the 400 μA focal spot. The hollow bars represent the un-neutralized focus, while the solid gray bars represent the result of using the filament to neutralize the focus.

simulated using the particle in cell code LSP. This code was written to study the interaction of a heavy ion beam with the wide range of gas and plasma densities that could occur in the target chamber.[19,20] For the purposes of modeling the introduction of electrons into the experiment, the code was run in a 2D, axisymmetric, electrostatic mode, with the electrons provided by space charge limited emission from a 12 mm radius disk at the beam entrance plane. In order to model

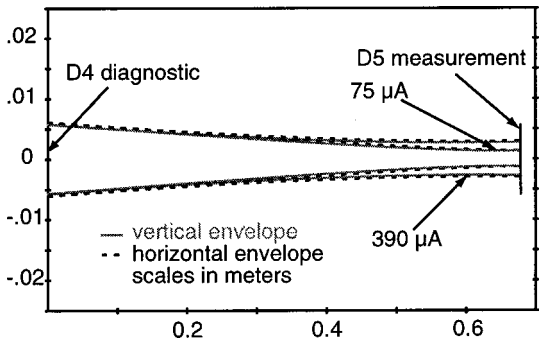

FIG. 11. Calculated beam envelopes between the last quadrupole magnet and the focus for both the neutralized and un-neutralized cases.

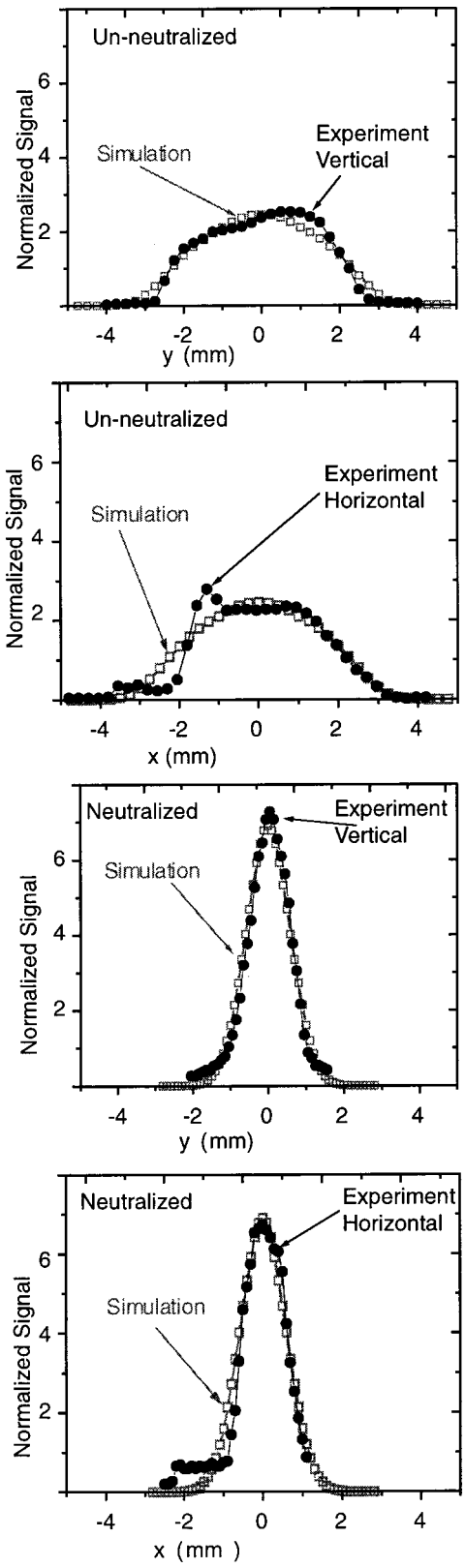

FIG. 12. The neutralized beam from the LSP run is plotted as it would be seen in a single slit scan. These data are compared to the measured spot.

the filament's ample supply of electrons, the field emission threshold was set to 0.01 V/cm, much lower than the self-fields within the beam.[19,21]

The simulation region is 120 cm in length and is surrounded by a conducting boundary at 3 cm, a factor of 5 larger than the maximum beam radius. An axisymmetric current density profile with radial variation based on a current density measurement at the exit of the last magnet was used at $z=0$. At the entrance plane, the ions were given the transverse velocity proportional to their radial position necessary to focus them at the axial location of the experimental measurements. Superposed on this is a thermal velocity contribution equivalent to a temperature of 0.18 eV, or 9 π mm mrad, corresponding to the measured emittance.

The results of the simulation[21] are presented in Fig. 12. To more accurately compare the output of the simulation with the experimental results, the charge density profile is projected onto one transverse dimension to emulate the diagnostic slit cup data. These projections are plotted on the same axes as the experimental data for the various measurements described in Sec. IV. The amplitudes of the curves in each plot are normalized such that their areas are equal, and the centroids of the experimental data are shifted to enhance the comparison. The extraordinary agreement between the curves suggests that the basic assumptions used to model the electron source were sound. The result also implies that the exact details of the initial beam distribution in both position and momentum space did not affect the ability of the electrons to produce a partially neutralized focus with an ion distribution on the target determined almost entirely by the beam emittance.

VI. CONCLUSION

The Scaled Final Focus Experiment at Lawrence Berkeley National Laboratory represents the first properly scaled study of the dynamics of the final focus of a heavy ion fusion driver. A beam of Cs^+ ions with perveance and convergence angles identical to those of the driver beam in the HIBALL-II report was brought to a focus in a system with a one-tenth dimensional scale of the design. Through measurements of the focal spot, it was determined that at least 80% of the beam particles fell within a 0.5 mm radius, meeting the scaled HIBALL-II requirement. Additionally, a source of electrons was introduced into a higher perveance beam to explore experimentally the properties of a neutralized focus. The measured focal spot was compared to beam envelope calculations that use reduced values of current to determine that the electrons neutralized 80% of the space charge at the focus. These measurements were also compared with a particle in cell simulation that included a mechanism for introduction of electrons. The resulting agreement benchmarks the theoretical approach and suggests that this type of neutralization may prove to be a satisfactory method for increasing the focal spot intensity of high perveance (i.e., $Q > 10^{-4}$) fusion driver beams.

ACKNOWLEDGMENTS

The authors gratefully acknowledge the outstanding support of the Lawrence Berkeley National Laboratory technical staff, including R. Beggs, W. Ghiorso, and R. Hipple.

This work was performed under the auspices of the Office of Fusion Energy Science, U.S. Department of Energy by Lawrence Berkeley National Laboratory under Contract No. DE-AC03-765F00098, and under the auspices of the U.S. Department of Energy by the University of California Lawrence Livermore National Laboratory under Contract No. W-7405-Eng-48.

[1]R. O. Bangerter, Nuovo Cimento Soc. Ital. Fis., A **106**, 1445 (1993).
[2]J. Hovingh, V. Brady, A. Faltens, D. Keefe, and E. P. Lee, Fusion Technol. **13**, 255 (1988).
[3]A. Garren, G. Krafft, and I. Haber, IEEE Trans. Nucl. Sci. **NS-28-3**, 2468 (1981).
[4]D. A. Callahan, Fusion Eng. Des. **32–33**, 441 (1996).
[5]S. Yu, S. Eylon, T. Fessenden, E. Henestroza, R. Lafever, W. Leemans, R. Petzoldt, D. Ponce, M. Vella, R. W. Moir, W. M. Sharp, R. Peterson, M. Sawan, and A. Tauschwitz, Nucl. Instrum. Methods Phys. Res. A **415**, 174 (1998).
[6]D. R. Welch, D. V. Rose, B. V. Oliver, T. C. Genoni, R. E. Clark, C. L. Olson, and S. S. Yu, Phys. Plasmas **9**, 2345 (2002).
[7]See National Technical Information Service Document No. DE86751390 (H. Wollnik, HIBALL-II: An Improved Conceptual Heavy Ion Beam Driven Fusion Reactor Study, KfK-3840, July 1985, pp. 57–71). Copies may be ordered from the National Technical Information Service, Springfield, VA 22161.
[8]J.-L. Vay and C. Deutsch, Nucl. Instrum. Methods Phys. Res. A **464**, 293 (2001).
[9]C. L. Olson, Nucl. Instrum. Methods Phys. Res. A **464**, 118 (2001).
[10]W. M. Sharp, D. A. Callahan-Miller, A. B. Langdon, M. S. Armel, and J.-L. Vay, Nucl. Instrum. Methods Phys. Res. A **464**, 284 (2001).
[11]I. M. Kapchinskij and V. V. Vladimirskij, in *Proceedings of the 1959 International Conference on High Energy Accelerators* (CERN, Geneva, 1959), pp. 274 ff.
[12]E. D. Courant and H. S. Snyder, Ann. Phys. (San Diego) **3**, 1 (1958).
[13]See National Technical Information Service Document No. ANL 79-41 (D. Neuffer, Proceedings of the Heavy Ion Fusion Workshop Held at Argonne National Laboratory September 19–26, 1978, ANL Rep. ANL-79-41, 1979, pp. 333–339). Copies may be ordered from the National Technical Information Service, Springfield, VA 22161.
[14]D. V. Rose, D. R. Welch, B. V. Oliver, R. E. Clark, W. M. Sharp, and A. Friedman, Nucl. Instrum. Methods Phys. Res. A **464**, 299 (2001).
[15]S. A. MacLaren, Ph.D. dissertation, University of California, Berkeley, 2000.
[16]M. Reiser, *Theory and Design of Charged Particle Beams* (Wiley, New York, 1994), pp. 379–390.
[17]S. Humphries, *Charged Particle Beams* (Wiley, New York, 1990).
[18]C. L. Olson, D. L. Hanson, J. W. Poukey, and D. R. Welch, Fusion Eng. Des. **32–33**, 485 (1996).
[19]D. R. Welch, D. V. Rose, B. V. Oliver, and R. E. Clark, Nucl. Instrum. Methods Phys. Res. A **464**, 134 (2001).
[20]T. P. Hughes, S. S. Yu, and R. E. Clark, Phys. Rev. ST Accel. Beams **2**, 110401 (1999).
[21]D. V. Rose, D. R. Welch, and S. A. MacLaren, in *Proceedings of the Particle Accelerator Conference*, Chicago, Illinois, 18–22 June 2001 (Institute of Electrical and Electronics Engineers, Piscataway, NJ, 2001), p. 3002.